Rockfall-protection embankments – design concept and construction details

Merlons de protection contre les chutes de pierres - modèle de conception et d'exécution

Hofmann R.
Ziviltechnikerbüro Dr. Hofmann, Perchtoldsdorf, Austria

Vollmert L.
BBG Bauberatung Geokunststoffe GmbH & Co. KG, Espelkamp, Germany

Mölk M.
Geologische Stelle des Forsttechnischen Dienstes für Wildbach- und Lawinenverbauung, Innsbruck, Austria

ABSTRACT: In the past, protection embankments were often erected in situations in which high design energies were anticipated; it was assumed that these embankments, if constructed appropriately, would provide adequate protection for such load cases. Rockfall-protection embankments are favoured in cases where the slope geometry and the space available allow their construction. In comparison with rockfall-protection nets, whose capacity to absorb energy is currently limited to 8000 kJ, embankments have advantages in terms of longevity, construction costs, and – depending on the construction – energy-absorbing capacity. To describe the failure mechanism associated with a dynamic impact on such an embankment, and to develop a design approach, model testing was carried out on conventional soil embankments, on reinforced embankments, and on embankments with stone facings. The objective of these model tests was to investigate the effects of rock impact on built-up embankments of various types, and to develop a concept for their design.

RÉSUMÉ : Dans le passé, les merlons de protection étaient souvent construits à haute énergie en supposant que ces merlons aient une capacité suffisante pour ces cas de chargement. Les merlons de protection contre les chutes de blocs sont construits, de préférence, dans les cas où la géométrie du talus et l'espace disponible permettent un tel ouvrage. En comparaison avec des filets protection contre les chutes de blocs, dont la capacité d'absorption d'énergie est actuellement limitée à 8000 kJ, les merlons ont des avantages, notamment en termes de durabilité, de coût de construction et - selon l'ouvrage - de capacité d'absorption d'énergie. Afin de décrire les surfaces de rupture des merlons causées par un impact dynamique et pour la mise en place d'une approche de conception, des modèles expérimentaux ont été réalisés avec des merlons en sol pur, des merlons renforcés et merlons en sol avec un parement en pierres. L'objectif du projet pilote était d'étudier les effets des éclats de blocs sur les différents types de merlons et de développer un dimensionnement.

KEYWORDS: rockfall protection, embankments, impact, energy absorption, design, model test, prototype, geosynthetics

1 INTRODUCTION

In the virtual absence of design rules for dynamic actions on pure soil structures, in the past 15 years designers have often resorted to the use of concepts used in the design of rockfall-protection galleries. The required parameters were derived from model testing (and, in a few cases, from full-scale tests) carried out since the late 1990s mainly in Switzerland, Austria, Italy and France (Blovsky (2002), Labiouse & Heidenreich (2009), Lambert et. Al (2011), Peila (2007) and Pichler et al. (2005)) In some cases, numerical calculations (Peila (2007) and Plassiard & Donze (2010)) were performed. In contrast to a rockfall-protection embankment, a rockfall-protection gallery is a stiff, reinforced-concrete construction overlain by a cushioning layer of various materials with differing thicknesses.

The construction of protection embankments has increased markedly in areas with a high risk of rockfall. No suitable design models for soil embankments currently exist which enable a geotechnical assessment of the stability of such structures. 1g model tests were therefore performed to obtain a picture of the failure mechanism under impact forces, and to use this to devise a design model.

A total of 150 tests with different structures (soil embankments, reinforced embankments, embankments with rip rap facing, embankments with cushioning elements), cross-sectional profiles, impact angles, freeboards, and impact energies were performed. The length of the embankment, and its height, were kept constant in all the tests. Several significant parameters have been varied, see 2.2. The test series were complemented with model embankments with rip rap facing and cushioning elements, and with geosynthetics. The model-scale geosynthetics were manufactured and delivered by NAUE.

2 SCALED MODEL TESTS

2.1 *Model tests*

The tests serve as experimental model tests, and the questions to be answered are limited to the shape of the failure body created in an embankment by a dynamic impact. A model scale of 1:33 was chosen to correspond to the energy involved in practice. The objective of these qualitative model tests was to depict with model embankments in the laboratory the failure mechanism generated in embankments by rock impact, see Hofmann & Mölk (2012).

The sphere was impacted against the embankment at three velocities (v1 = 4,5 m/s, v2 = 3,5 m/s, v3 = 6,0 m/s). Using the model scale of 1:33, these correspond to velocities of: v1 = 25,8 m/s, v2 = 20,1 m/s, v3 = 34,4 m/s in real life. The plastic displacements in the embankment and the penetration depth of the sphere were measured after each impact at two levels using several model extensometers (Figure 1).

2.2 *Structure types investigated*

Different slope angles β_{UPHILL} (4:5, 50°, 60° and 70°) and $\beta_{DOWNHILL}$ (2:3, 50°, 60° und 70°) and crest widths (b_1 = 2,5 cm, b_2 = 5,0 cm, b_3 = 10 cm and b_4 = 20 cm) were investigated and the impact height of the sphere (measured along the slope from the lowest point of the sphere up to the crest h_1 = 8 cm, h_2 = 16 cm, h_3 = 12 cm and h_4 = 20 cm) was varied.

Property	Unit	$F_{M,k}$ GGR_LS	λ	$F_{P,k}$
		Geogrid		Geogrid
Tensile strength md	kN/m	0.25	1089	272.3
Extension ε, md	%	5	-	5
Tensile strength cmd	kN/m	0.14	1089	152.5
Extension ε, cmd	%	5	-	5

Table 1: Tensile properties of the model geosynthetics

Property	Unit	GGR_LS	GTX_A
		Geogrid	Nonwoven
Mass per unit area	g/m²	28	39
Thickness	mm	0.24	0.25
Tensile strength md	kN/m	0.25	0.36
Extension ε, md	%	5	16
Tensile strength cmd	kN/m	0.14	0.09
Extension ε, cmd	%	5	55

Table 2: Conversion of characteristic strength properties model/prototype (Index k: characteristic)

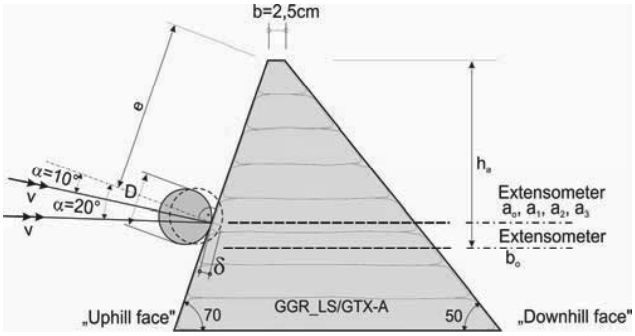

Figure 1. Cross section with extensometers

2.3 *Model embankments with geosynthetics*

The model embankment was reinforced with geosynthetics GGR_LS and GTX_A supplied by NAUE (Table 1).
If the model laws are observed, then a line load in this model has a transfer factor $\lambda^2 = 33^2 = 1089$ [-]. The characteristic values given in Table 2 are derived using this and equate to the full-scale values characteristic for the prototype.at a scale of 1:1.

The effective tensile strengths in the model are obtained using a factor of A2 = 1.2 for installation damage resulting from sub-base placement and compaction, as are the strengths $FP_{,d}$ relevant for the prototype after application of all reduction factors e.g. installation damage (Table 3).

2.4 *Model embankments with stacked-rock facing*

In some tests, a rip rap facing was used on the uphill face of the embankment (Figure 2).

Property	Unit	$F_{P,d}$	$J_{P,d@5\%}$
		Geogrid	
Tensile strength md	kN/m	226.9	4538
@ Extension ε, md	%	5	-
Tensile strength cmd	kN/m	127.1	2542
@ Extension ε, cmd	%	5	-

Table 3: Required values for reinforcement of the prototype (Index d: design)

3 BASIS FOR DESIGN MODEL

3.1 *Evaluation using relative impact energy and penetration depth*

In the model tests, the size and shape of the failure body created by the sphere were recorded. With the help of a non-dimensional evaluation of the test results, diagrams were drawn up to enable the results to be transferred to the full-scale situation, Hofmann & Mölk 0.

For the evaluation, an activated soil body was defined near the embankment crest (Figure 3). A non-dimensional depiction of the results is shown in Figure 4. The relative impact energy E* was introduced and plotted against the non-dimensional value δ/b, where δ is the depth of penetration of the sphere into the embankment and b is the crest width. The upper extensometers (a_0, a_1, a_2, a_3) were positioned at the mid-point of the sphere in the axis of the embankment; one extensometer was positioned at the level of the bottom of the sphere. The following variables are introduced:

$$E^* = E / (\gamma * A_a * D * h_a) \text{ (-)} \quad (1)$$
$$E = m\, v^2/2 \text{ (Joule)} \quad (2)$$
$$\gamma = \rho * g \text{ (N/m}^3\text{)} \quad (3)$$
$$A_a = (b+c)/2 * h_a \text{ (activated area) (m}^2\text{)} \quad (4)$$

where E* is the relative impact energy, m is the mass of the sphere in kg, v its velocity in m/s (v_1;v_2;v_3), ρ the soil density in kg/m³, g the gravitational acceleration in m/s², D the diameter of the sphere in m, h_a the activated height in m and b the crest width in m.

3.2 *Lessons learned from the tests*

3.2.1 *Lessons from the model tests for all construction types*

- In the vicinity of the impact, the body of the embankment undergoes significant compaction, and the crest is displaced upwards.
- The slimmer the construction, the larger the failure body on the downhill face of the embankment.
- A comparison of the different model tests clearly shows the more pronounced elasto-plastic behaviour of the embankment reinforced with geogrids compared with the unreinforced case (Figure 4).

3.2.2 *Lessons from trials without rip rap facing and without geosynthetics*

- A comparison shows how the deformations increase significantly from the lowest point of the sphere upwards. Observation of the model tests shows that a freeboard of at least twice the diameter D of the sphere

is required to prevent the sphere rebounding over the embankment crest on the first impact.

- The maximum width of the activated embankment body is 5 to 6 times the sphere diameter.
- In the tests it was found that the failure planes from the second impact onwards tended increasingly to form in an upward direction.
- The pictures taken with the high-speed camera clearly show quite significant elastic deformations during the period of impact.

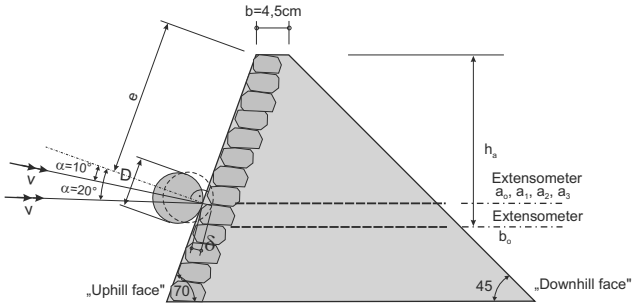

Figure 2. Model embankment with rip-rap facing

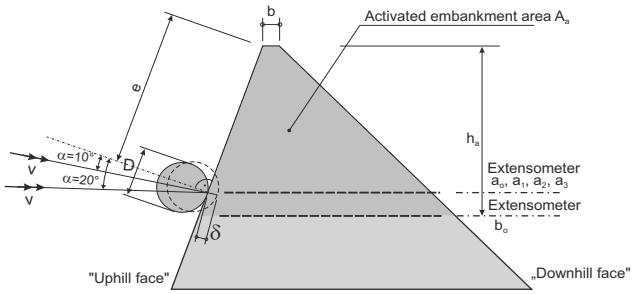

Figure 3. Model embankment system

3.2.3 Lessons from trials with rip rap facing and without geosynthetics

The following additional observations were made on embankments with rip rap facing:

- Slope angles ≥ 50° require a freeboard of at least 1 x the diameter of the sphere.
- After the impact, the sphere scarcely changes its height, whereas in the case of pure soil embankments, and reinforced structures, it tends to jump or roll in the direction of the crest.

3.2.4 Lessons learned from the tests with geosynthetics

- The model tests with the geosynthetics all showed a significantly larger lateral distribution (influence width) of the displacements. An influence width of at least 8 - 9 times the diameter of the sphere can be estimated from the measurements and the pictures taken with the high-speed camera.
- Very slim constructions with uphill and downhill slope angles of 70° and 60° were also investigated. These exhibited a noticeably more elastic behaviour than pure soil embankments.
- However, they require a markedly greater freeboard than embankments with rip rap facing. For geogrid-reinforced structures, a freeboard of 1.5 times the sphere diameter can be considered as being on the safe side.

4 DESIGN MODEL FOR ROCKFALL-PROTECTION EMBANKMENTS

4.1 *Principles*

A characteristic failure body for different structures was derived from the 1g model tests. An important and consistent parameter was the activated width of the embankment in the direction normal to the impact. The basic concept of the proposed design method is to derive a non-dimensional relationship between the penetration depth and the crest width (δ/b) using the relative impact energy E*, Hofmann & Mölk (2012).

4.2 *Activated failure body*

Normal to the impact direction, the size of the activated failure body is a function of the embankment structure. Whereas the width of the failure body in unreinforced embankments (both with and without rip rap facing) is at least 5 to 6 times the diameter of the block (the sphere in the model), this value increases to 8 to 9 times the diameter of the block for reinforced structures.

4.3 *Required freeboard*

Freeboard is defined here as the distance between the upper surface of the block and the upper surface of the embankment, measured along the slope (Section 3.2)

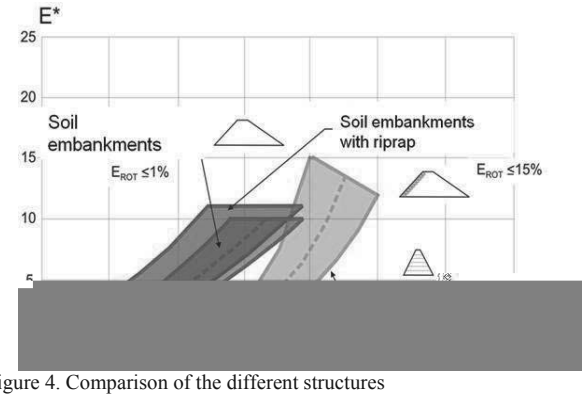

Figure 4. Comparison of the different structures

4.4 *Estimate of the equivalent static force*

An estimate of the equivalent static force is made using equation (5), on the assumption that the force initially increases, and then decreases, in a linear manner, and that the velocity decreases in a linear manner according to Blovsky (2002) (Figure 5). The equivalent static force is then distributed over the activated embankment width involved.

$$F = v^2 \, m / \delta \quad (5)$$

$$F = 2 \, v \, m / \Delta t \quad (6)$$

$$\Delta t = 2 \, \delta / v \quad (7)$$

$$\delta = (0{,}8 \text{ bis } 0{,}85) \, m \, v^2 / F \quad (8)$$

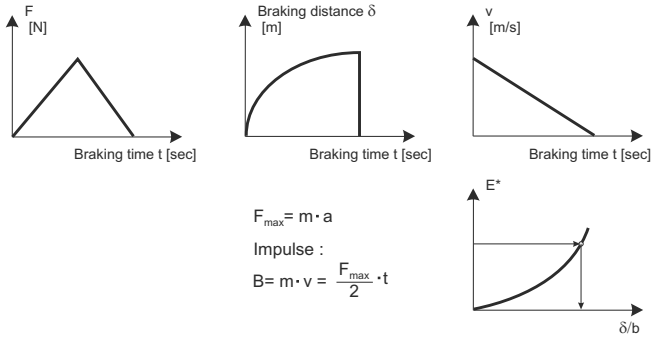

Figure 5. Assumptions for the evaluation (a = deceleration)

4.5 *Structure configuration*

The constructive aspects of rockfall-protection embankments are just as important as their numerical design. Rockfall incidents inevitably result in damage and wear on the facing. If at all possible, the facing should therefore effectively protect the outer surface of the reinforced earth body; it should also require little maintenance and ideally allow inspection, in case partial damage requires repair (ONR 24810 (2013) und ÖNORM B 1997-1-1 (2007)).

If rockfall-protection embankments are constructed as reinforced-soil bodies with steep side slopes, the reinforced body must have a wrap-round front surface to guarantee adequate anchorage for individual reinforcing layers at the edge of the structure. A facing is required to protect the structure against UV and impact. Figure 6 shows an example of a slim gabion solution which allows inspection and can be built independently of the supporting embankment body. The thickness, the area weight of the protective layer, and the quality of the steel elements must reflect the anticipated stressing/loading.

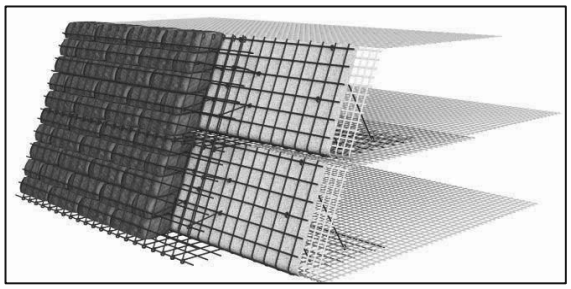

Figure 6. Inspectable outer facing-system (double-wall-system) to protect the load-bearing structure built using the wrap-around method (System NAUE DW)

5 COMPARISON OF DESIGN MODEL WITH FULL-SCALE TESTS

The results of model testing form the basis for the application of the results to full-size construction. To investigate the applicability of the design proposal, it will be necessary to evaluate existing protection embankments and the damage observed to have resulted from rockfall. This means that, after an incident, at the very least the block size and the penetration depth will have to be documented. Additionally, the velocity will have to be back-calculated using a rockfall-impact simulation program. The diagram in Figure 4 was confirmed at least by the full-scale tests of Peila et al. (2007), Lambert et al.(2011), and the observations of protection embankments in Tirol and Voralberg. The comparisons of observations on actual structures with the results obtained using the design proposals are summarised in Table 4. It can be seen that there is very good agreement.

Table 4: Comparison of full-size tests with design proposal

9 REFERENCES

Blovsky S. (2002). Reinforcing possibilities with geosynthetics Dissertation. Technische Universität Wien. Institut für Grundbau- und Bodenmechanik.

Labiouse V. and Heidenreich B. (2009). Half-scale experimental study of rockfall impacts on sandy slopes. - Nat. Hazards Earth Syst. Sci. 9, pp. 1981–1993.

Lambert S., Heymann A. and Gotteland P.(2011). Real-scale experimental assessment of cellular rockfall protection structures. Proceedings interdisciplinary workshop on rockfall protection – ROCEXS, Innsbruck 2011.

Peila, D., Oggeri, C. and Castiglia, C. (2007). Ground reinforced embankments for rockfall protection: design and evaluation of full scale tests. Landslides 4, pp. 255-265.

Pichler B., Hellmich C., and Mang H. (2005). Impact of rocks onto gravel – design and evaluation experiments. – International Journal of Impact Engineering 31, pp. 559-578.

Plassiard J.P. and Donze F.V. (2010). Optimizing the design of rockfall embankments with a Discrete Element Method. Engineering Structures, 32, pp. 3817-3826.

Hofmann R. und Mölk M. (2012). Bemessungsvorschlag für Steinschlagschutzdämme. Geotechnik 35, Heft 1, Verlag Ernst & Sohn.

ONR 24810 (2013). Technischer Steinschlagschutz – Begriffe, Einwirkungen, Bemessung und konstruktive Durchbildung, Überwachung und Instandhaltung(Technical protection against rockfall –Terms and definitions, effects of actions, design, monitoring and maintenance) Entwurf, Ausgabedatum: 2013-01-01.

ÖNORM B 1997-1-1 Eurocode 7 - Entwurf, Berechnung und Bemessung in der Geotechnik - Teil 1 (2007). Allgemeine Regeln - Nationale Festlegungen zu ÖNORM EN 1997-1 und nationale Ergänzungen.